Duncan, R. A., Backman, J., Peterson, L. C., et al., 1990
Proceedings of the Ocean Drilling Program, Scientific Results, Vol. 115

35. GEOCHEMISTRY OF PERIPLATFORM CARBONATE SEDIMENTS, LEG 115, SITE 716 (MALDIVES ARCHIPELAGO, INDIAN OCEAN)[1]

Mitchell J. Malone,[2] Paul A. Baker,[2] Stephen J. Burns,[3] and Peter K. Swart[3]

ABSTRACT

Site 716 is a continuous sequence (upper Miocene to Holocene) of periplatform oozes and chalks from the Maldives Ridge, Indian Ocean. Mineralogical and geochemical studies of these carbonate sediments indicate that submarine burial diagenesis has played an important role in the induration of sediments at this site. Metastable carbonates, high-magnesium calcite (HMC) and aragonite, convert to low-magnesium calcite (LMC) rapidly, within 1.1 and 6.0 Ma, respectively. Strontium concentrations in carbonate decrease with depth as the result of the burial diagenesis of calcium carbonate, primarily aragonite, with excess strontium being expelled into pore waters. The formation of celestite at depth indicates that sufficient diagenesis of carbonate sediments has occurred to saturate or supersaturate pore waters with respect to this authigenic mineral. Sodium also decreases monotonically with depth as a result of the burial diagenesis of calcium carbonate.

Magnesium and carbon and oxygen isotopic curves are remarkably similar. Carbon isotopic compositions record inputs of ^{13}C-enriched components from shallow carbonate banks. Magnesium concentrations vary widely, recording enhanced episodes of cementation by LMC with slightly elevated magnesium contents. Positive shifts in oxygen isotopic composition also record episodes of cementation during burial diagenesis. Intervals with increased accumulation rates of metastable components have undergone more rapid diagenesis than intervals with predominately pelagic deposition.

INTRODUCTION

Periplatform oozes are transitional carbonate deposits found between carbonate banks and the deep ocean (Schlager and James, 1978). Mineralogically, they are a mixture of bank-derived sediment, primarily high-Sr aragonite and high-magnesium calcite (HMC) (>4% $MgCO_3$), plus pelagic ooze composed of primarily low-magnesium calcite (LMC) coccoliths and foraminifers (Schlager and James, 1978). In addition, low-Sr aragonite pteropods can be an important component. The periplatform setting provides an ideal environment to study the potentially rapid diagenetic alteration of metastable carbonate minerals in marine carbonate sediments. As noted by previous investigators, the more intensely studied deep-sea monomineralic pelagic oozes are not representative of many ancient limestones (Schlager and James, 1978; Baker, 1981). The submarine diagenesis of periplatform sediments provides a modern example of how many Paleozoic shelf and slope limestones formed. These deposits probably formed by the accumulation and subsequent diagenetic alteration of aragonite and HMC in shallow subsiding basins subjected to little freshwater diagenesis. The evolution of LMC pelagic organisms in the Mesozoic heralded a decrease in the importance of shallow-water limestones. Consequently, the study of the diagenesis of periplatform sediments may provide geologists with insight into the lithification of ancient limestones.

Previous studies of periplatform oozes have been located primarily in the Bahamas (Kier and Pilkey, 1971; Droxler et al., 1983; Boardman and Neumann, 1985; Boardman et al., 1986; Burns and Neumann, 1987; Droxler et al., 1988). These studies have concentrated principally on sedimentological aspects of these deposits. Diagenetic studies of the Bahamian sediments include those of Schlager and James (1978), Mullins et al. (1980, 1985a), Dix and Mullins (1988a, 1988b), and Swart and Guzikowski (1988) (the only previous study of periplatform pore-water chemistry). Site 716 of ODP Leg 115 is one of only a few such periplatform sites ever drilled (the others were on ODP Leg 101 in the Bahamas). It is also the best of those sites in terms of having a nearly constant sedimentation rate and continuous recovery. Thus, Site 716 provides an excellent opportunity to increase our understanding of the diagenetic alteration of these sediments.

Site 716 is located in the Indian Ocean at 4°56.0′N and 73°17.0′E in a water depth of 543 m. The site is situated in a broad, shallow basin on the Maldives Ridge between the double atoll chain of the Maldives Archipelago (Fig. 1). The basin is filled with about 2.2 km of sediments and sedimentary rocks. The site is located in the center of the chain about 20–30 km from the present-day banks. Hole 716B is a 264.4-m hydraulic piston core with 100% recovery. The core contains a continuous, apparently uninterrupted late Miocene to Holocene sedimentary record (Backman, Duncan, et al., 1988). It consists of a homogeneous and monotonous sediment; olive, and pale olive to olive grey in color with no distinct turbidite layers. The color changes are gradational and bioturbation is seldom observed. Generally, the sediments are foraminifer-bearing nannofossil oozes, with pteropods and aragonite needles occurring abundantly in the upper part of the core. The pteropods become less abundant downcore and have essentially disappeared by approximately 54 m below seafloor (mbsf; 1.4 Ma).

Sedimentation rates based on nannofossil datum levels are 56 m/m.y. for the late Miocene and early Pliocene, 22–23 m/m.y. for the late Pliocene, and 38 m/m.y. for the Pleistocene (Backman, Duncan, et al., 1988). This study will attempt to resolve the timing and nature of cementation at Site 716 by determining the chemical composition and isotopic signature of sediments and chalks at this site.

METHODS

The core was sampled throughout its entire length at 50-cm intervals. In addition, samples of prominent chalk and celestite

[1] Duncan, R. A., Backman, J., Peterson, L. C., et al., 1990. *Proc. ODP, Sci. Results,* 115: College Station, TX (Ocean Drilling Program).

[2] Department of Geology, Duke University, P. O. Box 6729, College Station, Durham, NC 27708, U.S.A.

[3] Rosenstiel School for Marine and Atmospheric Sciences, Department of Geology and Geophysics, University of Miami, 4600 Rickenbacker Causeway, Miami, FL 33149, U.S.A.

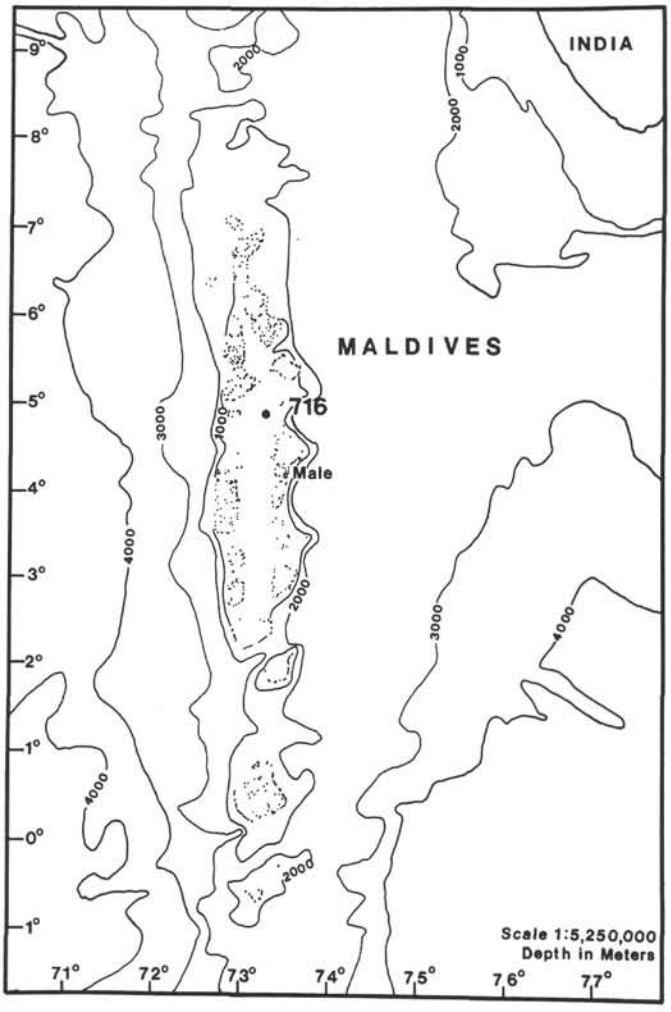

Figure 1. Location of Site 716.

nodules were taken. Chalks were identified by the methods of Gealy et al. (1971). According to their descriptive classification, chalks are firm or friable sediments that can be scratched with a fingernail or the edge of a spatula blade, whereas oozes have little strength and are easily deformed under the pressure of a finger or the broad blade of a spatula. This method was subjective and certainly some chalks could have been overlooked.

Approximately 550 samples were subjected to the following analyses. About 1 g of each sample was rinsed twice with distilled water, centrifuged, dried at 110°C, and powdered. One fraction was used to determine mineralogy on 154 selected samples by powder X-ray diffraction using a Phillips X-ray diffractometer with Cu-Kα radiation. Integrated peak area ratios of aragonite and calcite (low-Mg and high-Mg) were used to calculate their relative percentages vs. a standard calibration curve, as suggested by Milliman (1974). The LMC and HMC peaks were split following Milliman's technique (1974). The precision of these analyses was better than 5%. A second fraction of each sample was leached in acetic acid buffered by ammonium-acetate (pH = 5.5) for approximately 1 hr. The liquid was decanted and analyzed for calcium, magnesium, strontium, and sodium by flame atomic absorption spectrometry on a Perkin-Elmer Model 5000 spectrophotometer. Replicate analyses yielded results within 2% for wt% calcium carbonate, 4% for strontium and sodium, and 8% for magnesium.

About 50 buffered acetic acid-insoluble residues were analyzed by X-ray diffraction (XRD). A third fraction of bulk sediment was analyzed for carbon and oxygen isotopes on 112 selected samples at the University of Miami Rosenstiel School for Marine and Atmospheric Sciences on a Finnegan Mat-251 stable isotope ratio mass spectrometer. Isotopic values are reported as per mil (‰) deviations from the PDB standard. Sample extractions were performed in an on-line automated device that reacts the sample with 100% phosphoric acid at 90°C for 20 min. External error, determined by analyses of 20 replicate standards, is ± 0.026‰ for $\delta^{18}O$ and ± 0.016‰ for $\delta^{13}C$. In addition, selected bulk samples were studied by scanning electron microscopy on a JEOL T20 scanning electron microscope (SEM).

RESULTS

Mineralogy

Authigenic chalks become abundant below 70 mbsf, and authigenic celestite nodules appear commonly below 100 mbsf. Chalk is found in discrete layers or nodules (albeit not always obvious), but not in continually increasing abundance downcore. Much of the lower part of the core has a crusty texture that is intermediate between an ooze and a chalk.

Mineralogically, the uppermost sediment is a mixture of LMC, HMC, and aragonite (Fig. 2). Acid-insoluble residues are principally celestite, quartz, clay minerals, and dolomite. The buffered acetic acid leach used in the elemental analysis does not significantly dissolve dolomite, leaving it as an insoluble residue. Dolomite is present in such low quantities (<1%) that it is not recognizable in XRD patterns of bulk samples. This finding is in contrast with studies of Bahamian periplatform sediments in which dolomite is often present in quantities as high as 15% of the fine fraction (Mullins et al., 1985b; Droxler et al., 1988). Of the 51 acid-insoluble residues analyzed, dolomite is present in 38. Dolomite is found as shallow as 26 mbsf and in intervals of high and low magnesium values.

The dominant mineralogy throughout the core consists of LMC. Aragonite and HMC have their greatest abundances in the upper part of the core. Furthermore, HMC is present only in minor quantities, with a maximum of only 10% in the total carbonates in the upper 1 mbsf (compared with 17% of the fine fraction; Droxler et al., this volume). Below 32 mbsf (1.1 Ma), HMC is absent, and it is not found again in the lower sections. Aragonite is a significant component in the upper 60–70 m (1.9–2.3 Ma), varying from 15% to 40% of the total carbonates (the fine fraction in this interval ranges from 40% to 80% aragonite; Droxler et al., this volume). The aragonite content decreases to <10% by 100 mbsf (3 Ma), increases slightly to ~15% at 130 mbsf (4.25 Ma), and then decreases to <6% until it finally disappears by 250 mbsf (6 Ma). Eight discrete celestite nodules were identified, the shallowest appearing at 111.6 mbsf (3.4 Ma). Celestite, apparently not occurring as discrete nodules, was found at 124.4, 133.1, 142.6, 177.7, 200, 206.7, and 219.3 mbsf.

Minor Elements

Results of elemental analyses are reported in Table 1. Calcium is reported as wt% calcium carbonate; all other elements are reported as ppm in calcium carbonate. Carbonate content varies from 85% to 98%, increasing gradually downcore (Fig. 3). During the last 2 Ma (about the upper 60 mbsf), the calcium carbonate content is related to sea-level cycles (Fig. 4). The wt% calcium carbonate is higher during highstands (interglacials), whereas the % coarse fraction and $\delta^{18}O$ are lower (Droxler et al., this volume).

Strontium concentrations fluctuate considerably above 60 mbsf, with values ranging from 2200 to 4000 ppm of the total carbonate fraction (Fig. 5). Over the next 40 m, strontium concentrations gradually decline to approximately 1600 ppm, and

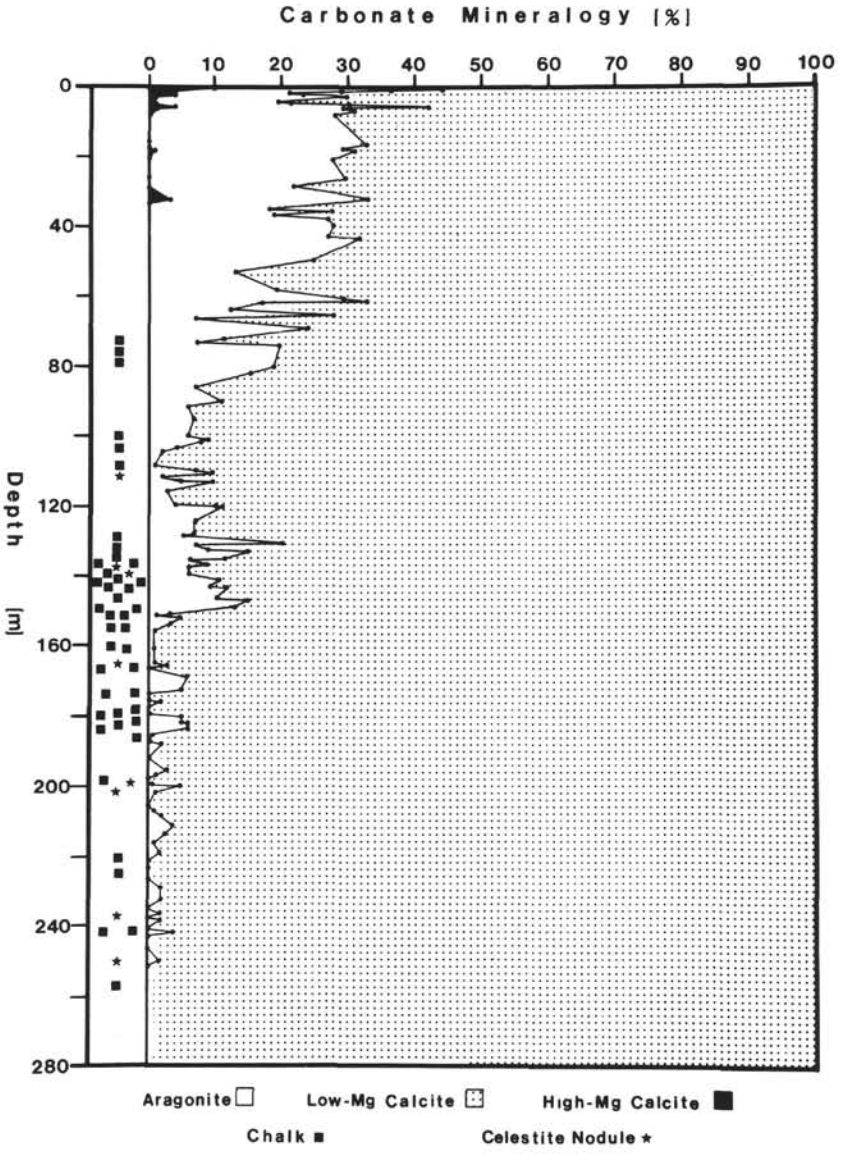

Figure 2. Relative % carbonate mineralogy. Solid squares = chalks and stars = celestite nodules.

they remain nearly constant throughout the rest of the core. Anomalously high strontium values below 100 mbsf are primarily caused by samples that contain small amounts of celestite (some celestite dissolves during dissolution). Milliman (1974) and, later, Boardman and Neumann (1984) have shown that bank-derived aragonite is more enriched in strontium than pelagic aragonite and calcite. The proportion of aragonite in the upper 60 mbsf implied by end-member mixing can be approximated by

$$(X)(7000 \text{ ppm}) + (1 - X)(1600 \text{ ppm}) = \text{observed ppm} \quad (2200 - 4000),$$

where X = the proportion of high-Sr aragonite. End-member concentrations of strontium are taken to be 7000 ppm in high-Sr aragonite and 1600 ppm in low-Sr aragonite. This calculation suggests that high-Sr aragonite makes up 11%–44% of the bulk carbonate between 0 and 60 mbsf, which agrees well with percentages determined by XRD. We attribute the variability of strontium concentrations observed in the upper 60 m to glacial-interglacial cycles in periplatform-derived aragonite. Strontium concentrations and aragonite contents are higher during interglacial periods (see Droxler et al., this volume). Aragonite cycles have previously been documented in periplatform sediments (e.g., Kier and Pilkey, 1971; Droxler et al., 1983; Boardman and Neumann, 1984; Boardman et al., 1986; Droxler et al., 1988) and are being studied further by Droxler et al. (this volume). A plot of strontium in this interval (Fig. 6) shows that high strontium values also generally coincide with high calcium carbonate (Fig. 4). There are, however, occasional exceptions.

Strontium concentrations have previously been shown to be an important indicator of diagenesis in carbonate sediments. Biogenic calcium carbonate is enriched in strontium with respect to diagenetic LMC, the end product of marine burial diagenesis. During diagenesis, biogenic calcite (both high and low magnesium) and aragonite recrystallize to inorganic LMC, and the excess strontium is released into the pore waters (Baker et al., 1982). We ascribe the downcore decrease of strontium in the

Table 1. Elemental and stable isotopic composition of bulk carbonate samples, Site 716.

Core, section, interval (cm)	Depth (mbsf)	$CaCO_3$ (wt%)	Mg (ppm)	Sr (ppm)	Na (ppm)	$\delta^{13}C$ (‰)	$\delta^{18}O$ (‰)
115-716B-							
1H-1, 10-12	0.1	88.6	5510	3890	2337	0.9	−1.95
1H-1, 50-52	0.5	86.6	6341	3353	2419		
1H-1, 110-112	1.1	87.2	4562	2357	2041		
1H-2, 10-12	1.6	84.9	4571	2994	2002		
1H-2, 50-52	2	87.3	5067	3376	2030	1.02	−0.97
1H-2, 110-112	2.6	88.6	5138	3544	1882		
2H-1, 10-12	4	86.4	2732	5107	1996		
2H-1, 50-52	4.4	86.3	5274	2605	1996		
2H-1, 110-112	5	88.9	4086	2466	1866	0.63	−0.38
2H-2, 9-11	5.49	94.2	3420	3027	2521		
2H-2, 50-52	5.9	92.2	4001	3336	2043		
2H-2, 110-112	6.5	85.9	4537	2889	1932		
2H-3, 10-12 (1)	7	93.1	4676	3958	2118	0.75	−1.26
2H-3, 10-12 (2)	7	93.3	4909	3904	2112		
2H-3, 10-12 (3)	7	92.4	5186	3722	2118		
2H-3, 50-52	7.4	90.1	4110	2561	1912		
2H-3, 110-112	8	87.8	4526	2751	1663		
2H-4, 10-12	8.5	93.6	4733	3520	1926		
2H-4, 50-52	8.9	94.4	3796	3513	1796		
2H-4, 110-112	9.5	93.1	3857	3218	1644	0.86	−1.06
2H-5, 10-12	10	91.6	3685	3031	1188		
2H-5, 50-52	10.4	86.9	2991	2962	1961		
2H-5, 110-112	11	89.7	3386	3226	1879		
2H-6, 10-12	11.5	90.5	3087	3353	2915		
2H-6, 50-52	11.9	93.3	2963	3261	1888	0.74	−1.21
2H-6, 110-112	12.5	89.4	3284	2791	1709		
2H-7, 10-12	13	87.8	3199	2532	1505		
3H-1, 50-52	14	91.7	2813	3151	1848		
3H-1, 110-112	14.6	93.6	2547	3126	1743	0.63	−1.32
3H-2, 10-12	15.1	88.1	3250	2788	1876		
3H-2, 50-52	15.5	92.6	3633	3006	3530		
3H-2, 110-112	16.1	88.1	3380	2284	1769		
3H-3, 10-12	16.6	87.9	3567	2662	1713	0.44	−0.67
3H-3, 50-52	17	91.9	2081	2907	1790		
3H-3, 110-112	17.6	93.8	2702	2390	1757		
3H-4, 10-12	18.1	91.7	3058	2273	1881		
3H-4, 50-52	18.5	89.8	3497	3475	3957		
3H-4, 110-112	19.1	90.8	3177	3149	1984	0.47	−1.09
3H-5, 10-12 (1)	19.6	92.2	3455	3152	1854		
3H-5, 10-12 (2)	19.6	91.9	3080	3298	1881		
3H-5, 10-12 (3)	19.6	90.7	2453	3303	1868		
3H-5, 50-52	20	90.5	3386	2782	1845		
3H-5, 110-112	20.6	94.1	3293	3713	1739	0.75	−0.8
4H-1, 10-12	23.2	91.4	2480	2567	1504		
4H-1, 50-52	23.6	87.3	2737	3296	2218		
4H-1, 110-112	24.2	88.1	2690	2915	1597	0.32	−2.28
4H-3, 10-12	26.2	92.1	2903	3411	2179	0.55	−0.87
4H-3, 50-52	26 6	90.9	2834	2834	1553		
4H-3, 110-112	27 2	90.6	2907	2808	1643		
4H-4, 10-12	27.7	90.5	3129	2687	1297		
4H-4, 50-52	28.1	89.6	2954	2904	1519		
4H-4, 110-112	28.7	89.3	3616	3007	1682	0.42	−0.42
4H-5, 10-12	29.2	92.1	4703	2671	1700		
4H-5, 50-52	29.6	97.2	4377	2593	1590		
4H-5, 110-112	30.2	92.8	4944	3336	1764		
4H-6, 10-12	30.7	91.6	5179	3363	1725		
4H-6, 50-52	31.1	95.4	5063	3099	1733	0.85	−1.28
4H-6, 110-112	31.7	91.6	5293	3725	1822		
5H-1, 10-12	32.9	93.9	2575	3214	1641		
5H-1, 50-52	33.3	87.3	2942	2914	2919		
5H-1, 110-112	33.9	90.6	2363	2517	1363	0.59	−1.04
5H-2, 10-12	34.4	90.3	2187	2490	1363		
5H-2, 50-52	34.8	92.7	2195	3390	1681		
5H-2, 110-112	35.4	93.9	2505	3617	6314		
5H-3, 10-12	35.9	94.6	3063	3110	7084	0.34	−1.1
5H-3, 50-52	36.3	94.9	2338	3166	1504		
5H-3, 110-112	36.9	93.8	2596	3027	1548		
5H-4, 10-12	37.4	94.2	2813	3282	1588		
5H-4, 50-52	37.8	92.1	2746	3487	1768		
5H-4, 110-112	38.4	91.5	2834	3052	1575	0.51	−1.01
5H-5, 10-12	38.9	92.1	3036	3418	1706		
5H-5, 50-52	39.3	93.9	2880	3073	1775		
5H-5, 110-112	39.9	93.8	3223	3335	1782		
5H-6, 10-12	40.4	93.1	3596	3665	1697		
5H-6, 50-52	40.8	93.7	3660	3569	1771	0.96	−0.7
5H-6, 110-112	41.4	94.5	3505	3739	3314		
5H-7, 10-12	41.9	93.3	2814	3027	1569		
5H-7, 50-52	42.3	88.9	3216	4070	2623		
6H-1, 10-12	42.6	90.4	3794	3832	1706		
6H-1, 50-52	43	91.1	3505	3221	1553		
6H-1, 110-112	43.6	90.6	4391	3177	1550	0.64	−0.25

Table 1 (continued).

Core, section, interval (cm)	Depth (mbsf)	$CaCO_3$ (wt%)	Mg (ppm)	Sr (ppm)	Na (ppm)	$\delta^{13}C$ (‰)	$\delta^{18}O$ (‰)
115-716B- (Cont.)							
6H-2, 10-12	44.1	89.9	4656	3303	1530		
6H-2, 50-52	44.5	91.5	4914	3314	2833		
6H-2, 110-112	45.1	91.9	5228	3271	1811		
6H-3, 10-12	45.6	91.5	5071	3006	1449	0.99	0.11
6H-3, 50-52	46	91.8	5358	2930	2006		
6H-3, 110-112	46.6	93.2	4378	2505	1298		
6H-4, 10-12	47.1	94 5	5053	3000	1298		
6H-4, 50-52	47.5	89 9	4656	3425	1591		
6H-4, 110-112	48.1	91 4	4753	3341	1483	0.96	0.03
6H-5, 10-12	48.6	92.1	4714	3028	1481		
6H-5, 110-112	49	90.4	5359	3177	3633		
6H-6, 10-12	50.1	87.3	4345	3016	1517		
6H-6, 50-52	50.5	86.2	5067	3042	1599	1.03	0.37
6H-6, 110-112	51.1	93.6	4129	2719	1523		
6H-7, 10-12	51.6	88.7	4957	3267	1701		
6H-7, 50-52	52	91.5	4802	3200	1750		
7H-1, 10-12	52.2	86.6	5816	2737	1494		
7H-1, 50-52	52.6	90.9	4824	2954	1471		
7H-1, 110-112	53.2	92.3	3833	2741	1427	0.8	0.0
7H-2, 10-12	53.7	91.5	4385	3028	1341		
7H-2, 50-52	54.1	91.3	4661	3028	1462		
7H-2, 110-112	54.7	91.1	4166	2517	1407		
7H-3, 10-12	55.2	93.2	4707	3074	1468	1.02	0.08
7H-3, 50-52	55.6	93.5	2596	3615	1937		
7H-3, 110-112	56.2	90.7	3663	3151	1575		
7H-4, 10-12	56.7	91.3	3352	3516	1586		
7H-4, 50-52	57.1	89.8	3658	3647	3697		
7H-4, 110-112	57.7	90.7	3843	2933	1483	0.64	−0.12
7H-5, 10-12	58.2	93.8	4391	3378	1641		
7H-5, 50-52	58.6	91.9	4985	3125	1671		
7H-5, 110-112	59.2	91.8	4320	3174	1649		
7H-6, 10-12	59.7	94.7	3644	3235	1503		
7H-6, 50-52	60.1	92.8	4242	3100	1636	0.8	0.08
7H-6, 110-112	60.7	92.8	3362	3770	1764		
7H-7, 10-12	61.2	87.1	4111	3826	1625		
7H-7, 50-52	61.6	87.1	4202	3398	1608		
8H-1, 10-12	61.8	90.1	5105	2782	1175		
8H-1, 50-52	62.2	91.5	4693	2741	1233		
8H-1, 110-112	62.8	92.6	4548	2933	1893	0.95	0.1
8H-2, 10-12	63.3	96.4	4229	2567	1023		
8H-2, 50-52	63.7	90.6	3985	2786	1529		
8H-2, 110-112	64.3	93.3	4989	2410	957		
8H-3, 10-12	64.8	90.5	3930	2538	1120	0.9	0.21
8H-3, 50-52	65.2	91.7	3794	3418	1254		
8H-3, 110-112	65.8	91.7	3698	2330	1070		
8H-4, 10-12	66.3	93.6	5314	1840	957		
8H-4, 50-52	66.7	93.3	3952	2789	1266		
8H-4, 110-112	67.3	92.8	4108	2982	1094	0.87	0.37
8H-5, 10-12	67.8	92.6	4875	2644	1073		
8H-5, 50-52	68.2	93.2	4489	2787	1085		
8H-5, 110-112	68.8	91.9	3250	2719	1148		
8H-6, 10-12 (1)	69.3	91.4	3849	2665	1092		
8H-6, 10-12 (2)	69.3	93.8	3920	2649	1053		
8H-6, 10-12 (3)	69.3	93.3	3617	2553	1096		
8H-6, 50-52	69.7	95.6	2494	3030	1268	0.76	−0.72
8H-6, 110-112	70.3	90.5	3036	2448	1101		
8H-7, 10-12	70.8	93.9	3330	2296	1256		
8H-7, 50-52	71.2	94.3	2895	2136	1236		
9H-1, 10-12	71.5	95.9	3381	2221	1154		
9H-1, 50-52	71.9	95.1	5085	1750	893		
9H-1, 110-112	72.5	93.7	3631	1989	1150	0.48	0.24
9H 2, 10-12 (CH)	73	94 3	3581	1440	838	0.89	0.8
9H 2, 50-52	73.4	93.9	3008	2839	1414		
9H-2, 110-112	74	96 5	3546	1989	928		
9H-2, 10-12 (CH)	75.5	92 2	4263	1357	826	0.6	1.0
9H-3, 50-52	74.9	90.6	4864	2050	1055		
9H-3, 110-112	75.5	90.4	3897	2149			
9H-4, 10-12	76	96.9	2327	1861	1053		
9H-4, 50-52	76.4	91.3	3011	1941	962		
9H-4, 110-112	77	90.1	3177	3468	1709	0.13	−0.79
9H-5, 10-12	77.5	93.7	3504	2628	1361		
9H-5, 50-52 (CH)	77.9	92.9	3702	1532	793	0.63	0.86
9H-5, 110-112	78.5	92.1	3233	2546	1243		
9H-6, 10-12	79	87.3	3062	1568	867		
9H-6, 50-52	79.4	91.6	2968	2882	1254	0.31	−0.64
9H-6, 110-112	80	92.7	2793	2032	989		
9H-7, 10-12	80.5	91.6	2503	2665	1471		
9H-7, 50-52	80.9	93.1	3143	2596	1094		

Table 1 (continued).

Core, section, interval (cm)	Depth (mbsf)	$CaCO_3$ (wt%)	Mg (ppm)	Sr (ppm)	Na (ppm)	$\delta^{13}C$ (‰)	$\delta^{18}O$ (‰)
115-716B- (Cont.)							
10H-1, 10–12	81.2	92.6	3368	2379	1146		
10H-1, 50–52	81.6	93.6	2767	2596	1126		
10H-1, 110–112	82.2	96.2	2386	2149	1062	0.21	−0.88
10H-2, 10–12	82.7	92.2	2419	2499	1212		
10H-2, 50–52	83.1	91.3	3331	2539	1088		
10H-2, 110–112	83.7	84.6	2640	2236	1206		
10H-3, 10–12	84.2	87.4	3030	2007	995	0.44	−0.1
10H-3, 50–52	84.6	94.1	2701	2115	921		
10H-3, 110–112	85.2	93.1	2463	2101	1074		
10H-4, 10–12	85.7	89.7	2253	2001	1066		
10H-4, 50–52	86.1	96.4	3496	2400	1153		
10H-4, 110–112	86.7	92.1	1652	2202	1254	0.36	−1.6
10H-5, 10–12	87.2	93.3	1920	2362	1096		
10H-5, 50–52	87.6	93.7	2117	2245	957		
10H-5, 110–112	88.2	93.6	1681	2266	1287		
10H-6, 10–12	88.7	92.1	1823	2933	1459		
10H-6, 50–52	89.1	94.1	1710	2391	1224	0.27	−1.47
10H-6, 110–112	89.7	91.8	2195	2282	1070		
10H-7, 10–12	90.2	93.6	2223	2149	1085		
11H-1, 10–12	90.8	88.7	2359	1710	1062		
11H-1, 50–52	91.2	91.9	2371	1837	872		
11H-1, 110–112	91.8	84.2	2353	2154	1241	0.48	−1.0
11H-2, 10–12	92.3	93.1	2117	2218	1000		
11H-2, 50–52	92.7	92.1	2263	2097	997		
11H-2, 110–112	93.3	93.8	2359	2533	1055		
11H-3, 10–12	93.8	95.6	3236	2815	1122	0.49	−0.48
11H-3, 50–52	94.2	94.3	2939	2111	918		
11H-3, 110–112	94.8	92.8	2378	2388	1021		
11H-4, 10–12	95.3	94.9	2213	2239	1226		
11H-4, 50–52	95.7	93.9	2401	2459	1266		
11H-4, 110–112	96.3	93.9	2142	2860	2200	0.19	−1.27
11H-5, 10–12	96.8	94.3	2617	2322	1076		
11H-5, 50–52	97.2	93.5	3050	2153	929		
11H-5, 110–112	97.8	95.9	2852	1683	712		
11H-6, 10–12	98.3	92.1	3078	2188	799		
11H-6, 50–52	98.7	91.3	2836	2880	1198	0.34	−1.05
11H-6, 110–112	99.3	93.1	3711	2263	901		
11H-7, 10–12	99.8	95.2	3340	2306	852		
11H-7, 50–52	100.2	90.7	3265	2198	742		
12H-1, 10–12	100.4	91.2	3411	2546	1125		
12H-1, 50–52 (CH)	100.8	92.2	3030	1662	3405	0.18	−0.28
12H-1, 110–112	101.4	96.5	2409	2112	982		
12H-2, 10–12	101.9	92.6	2746	2429	987		
12H-2, 50–52	102.3	92.8	2245	2266	1074		
12H-2, 110–112	102.9	95.2	2382	1953	963		
12H-3, 10–12 (CH)	103.4	92.7	2335	3809	894	0.34	−0.85
12H-3, 50–52	103.8	95.3	2405	1610	841		
12H-3, 110–112	104.4	93.4	2420	1676	915		
12H-4, 10–12	104.9	95.7	2130	1543	831		
12H-4, 50–52	105.3	95.3	2403	1838	827		
12H-4, 110–112	105.9	93.9	2464	1710	960	0.13	−0.69
12H-5, 10–12	106.4	95.9	2493	1958	904		
12H-5, 50–52	106.8	95.7	2134	1850	1072		
12H-5, 110–112	107.4	95.1	2701	1764	1183		
12H-6, 10–12	107.9	95.1	2445	1811	911		
12H-6, 50–52	108.3	93.8	3029	1662	691	0.08	−0.37
12H-6, 110–112	108.9	96.5	2535	1510	855		
12H-7, 10–12 (CH)	109.4	97.3	2767	1406	798	0.13	−0.29
13H-1, 10–12	110.1	92.1	2768	2087	1049	0.21	−0.04
13H-1, 50–52	110.5	96.2	2324	1896	1031		
13H-1, 110–112	111.1	96.6	3002	1844	904		
13H-2, 10–12 (*)	111.6	77.1	3511	11789	3743		
13H-2, 50–52	112	92.7	2574	1957	809		
13H-2, 110–112	112.6	91.9	2834	1935	801		
13H-3, 10–12	113.1	90.4	3337	3475	1275	0.24	0.02
13H-3, 50–52	113.5	90.2	3287	1682	934		
13H-3, 110–112	114.1	91.9	3011	1800	1103		
13H-4, 10–12	114.6	92.1	3207	1711	1094		
13H-4, 50–52	115	93.1	2830	2245	1181		
13H-4, 110–112	115.6	94.7	2960	1377	939		
13H-5, 10–12	116.1	90.6	2567	2611	1621	0.47	0.27
13H-5, 50–52	116.5	90.3	3331	1852	835		
13H-5, 110–112	117.1	90.9	2616	1739	1068		
13H-6, 10–12	117.6	96.4	3058	1677	798		
13H-6, 50–52	118	95.8	2535	1704	1122	0.46	−0.67
13H-6, 110–112	118.6	95.7	2618	1797	956		
13H-7, 10–12	119.1	95.1	2487	1743	953		
13H-7, 50–52	119.5	91.7	2524	1570	894		
14H-1, 20–22	119.9	97.3	2651	1803	1710		

Table 1 (continued).

Core, section, interval (cm)	Depth (mbsf)	$CaCO_3$ (wt%)	Mg (ppm)	Sr (ppm)	Na (ppm)	$\delta^{13}C$ (‰)	$\delta^{18}O$ (‰)
115-716B- (Cont.)							
14H-1, 70–72	120.4	85.3	2991	2320	913	0.25	−0.39
14H-1, 120–122 (1)	120.9	91.3	4097	1958	3390		
14H-1, 120–122 (2)	120.9	91.4	3779	1936	801		
14H-1, 120–122 (3)	120.9	91.5	3806	2018	801		
14H-1, 120–122 (4)	120.9	93.4	3815	1986	777		
14H-2, 70–72	121.9	91.9	3063	1942	821		
14H-2, 120–122	122.4	93.1	2784	1862	826		
14H-3, 20–22	122.9	92.7	3618	1547	610		
14H-3, 70–72	123.4	92.5	3405	1619	680		
14H-3, 120–122	123.9	92.7	3083	2130	808		
14H-4, 20–22	124.4	90.9	3523	1764	1170	0.55	0.28
14H-4, 70–72	124.9	89.7	3374	1742	785		
14H-4, 120–122	125.4	94.5	3366	1659	685		
14H-5, 20–22	125.9	94.7	3701	1731	2640		
14H-5, 70–72	126.4	96.4	3321	1862	1320		
14H-5, 120–122	126.9	93.4	3702	1597	658		
14H-6, 20–22	127.4	89.8	3653	1991	920		
14H-6, 70–72	127.9	91.4	3565	1684	735	0.68	0.57
14H-6, 120–122	128.4	95.2	4082	1432	585	0.66	0.81
14H-7, 20–22	128.9	95.5	3779	1469	638		
14H-7, 70–72	129.3	90.5	3842	1840	714		
15H-1, 20–22	129.5	98.7	3401	1561	857		
15H-1, 70–72	130	93.2	3478	1710	627		
15H-1, 120–122	130.5	95.1	2734	2634	1070		
15H-2, 20–22 (CH)	131	93.5	3494	1694	712	0.83	0.9
15H-2, 70–72	131.5	96.4	3423	2531	887		
15H-2, 120–122	132	95.1	3908	1975	1380		
15H-3, 20–22 (CH)	132.5	95.9	3646	1781	695		
15H-3, 70–72	133	94.7	3492	2279	1040	0.61	−0.28
15H-3, 120–122	133.5	95.6	3630	1966	1020		
15H-4, 20–22	134	94.7	3695	2295	925		
15H-4, 70–72	134.5	93.9	3754	1954	733		
15H-4, 120–122	135	93.1	3715	2816	1170	0.79	0.05
15H-5, 20–22 (CH)	135.5	90.5	4347	1681	708		
15H-5, 70–72	136	94.8	3993	2172	897		
15H-5, 120–122	136.5	94.3	3859	2254	894		
15H-6, 20–22 (CH)	137	88.1	4021	3293	1220		
15H-6, 27–30 (CH)	137.07	94.3	4209	1623	1940	0.75	0.78
15H-6, 40–42 (*)	137.2	34.1	3916	58153	2240		
15H-6, 70–72	137.5	93.1	3831	1926	723		
15H-6, 120–122	138	93.6	4025	1809	707		
15H-7, 20–22	138.5	91.7	4205	1779	974		
16H-1, 20–22	139.1	94.5	3809	1659	716		
16H-1, 58-60 (CH)	139.48	93.7	3797	1513	1190	0.8	0.7
16H-1, 70–72	139.6	94.6	3809	2276	643		
16H-1, 120–122	140.1	96.2	4020	1621	700		
16H-2, 20–22	140.6	95.1	4036	1795	690		
16H-2, 70–72 (*)	141.1	42.6	3465	41793	1730		
16H-2, 120–122	141.6	97.9	3426	1885	816		
16H-3, 20–22 (CH)	142.1	93.5	3704	1649	664		
16H-3, 57-59 (CH)	142.47	95.9	3878	1568	967	0.85	0.78
16H-3, 70–72 (CH)	142.6	91.2	3922	3050	669		
16H-3, 107–109 (CH)	142.97	93.2	4301	1492	2140		
16H-3, 120–122 (CH)	143.1	93.6	4068	1584	1170		
16H-4, 70–72	144 1	96 8	3922	1817	818		
16H-4, 120–122	144.6	95.7	3993	1966	736		
16H-5, 20–22	145.1	93.5	4046	1593	765		
16H-5, 70–72	145.6	94.3	4225	1960	706		
16H-5, 120–122	146.1	96.7	4236	1760	669		
16H-6, 16–18 (CH)	146.56	96.4	4797	1565	1400	0.69	0.95
16H-6, 20–22	146.6	96.9	4253	1711	664		
16H-6, 70–72	147.1	94.8	4275	2013	786		
16H-6, 120–122	147.6	90.1	4231	1720	774		
16H-7, 20–22	148.1	93.5	3829	2156	844		
16H-7, 70–72 (CH)	148.6	88.1	4186	1962	751		
17H-1, 20–22	148.8	93.4	3855	1874	765		
17H-1, 70–72	149.3	93.2	4200	1651	658		
17H-1, 120–122	149.8	95.6	3507	2216	1100		
17H-2, 20–22	150.3	97.9	3682	1706	781		

Table 1 (continued).

Core, section, interval (cm)	Depth (mbsf)	$CaCO_3$ (wt%)	Mg (ppm)	Sr (ppm)	Na (ppm)	$\delta^{13}C$ (‰)	$\delta^{18}O$ (‰)
115-716B- (Cont.)							
17H-2, 70–72	150.8	95.1	3659	2357	936		
17H-2, 106-107 (CH)	151.16	96.1	4725	1469	998		
17H-2, 120–122 (CH)	151.3	94.7	4736	1364	653		
17H-3, 20–22 (CH)	151.8	94.1	4646	1434	573		
17H-3, 36–38 (CH)	151.96	94.4	4689	1412	961	−0.6	1.13
17H-3, 70–72	152.3	95.5	4320	1535	529		
17H-3, 120–122	152.8	97.1	3708	1613	612		
17H-4, 20–22	153.3	98.1	4014	1399	521		
17H-4, 70–72	153.8	98.4	3989	1343	562		
17H-4, 120–122	154.3	94.4	4147	1476	743	0.38	0.94
17H-5, 20–22	154.8	91.5	4569	1996	993		
17H-5, 70–72	155.3	95.5	4929	1432	596		
17H-5, 120–122 (CH)	155.8	94.2	3603	1322	664		
17H-6, 20–22 (CH)	156.3	97.5	3264	1476	756	0.6	0.7
17H-6, 70–72	156.8	96.9	3156	1762	863		
17H-6, 120–122	157.3	94.7	3288	1531	711		
17H-7, 20–22	157.8	95.9	3137	1613	633		
18H-1, 20–22	158.5	94.9	3314	1401	516		
18H-1, 70–72	159	92.8	3534	1559	648		
18H-1, 120–122	159.5	95.7	3178	1605	544		
18H-2, 20–22	160	96.9	3139	1662	546		
18H-2, 70–72 (1)	160.5	96.1	3195	1520	633		
18H-2, 70–72 (2)	160.5	96.8	3114	1508	587		
18H-2, 70–72 (3)	160.5	97.6	3155	1532	582		
18H-2, 70–72 (4)	160.5	94.7	3239	1556	605		
18H-2, 120–122	161	93.9	3238	1467	503		
18H-3, 20–22 (CH)	161.5	95.5	3573	1421	550	0.56	0.92
18H-3, 70–72 (CH)	162	95.7	3779	1375	810	0.52	1.0
18H-3, 120–122	162.5	95.8	3480	1421	477		
18H-4, 20–22	163	92.8	3774	1445	503		
18H-4, 70–72	163.5	94.5	4105	1354	510		
18H-4, 120–122	164	94.9	3711	1411	502		
18H-5, 20–22	164.5	94.9	3769	1923	596		
18H-5, 70–72	165	94 2	3590	1397	499	0.62	1.03
18H-5, 120–122	165-5	94.2	3685	1476	531		
18H-6, 8–11 (*)	165.88	30.9	2819	69218	2210		
18H-6, 20–22	166	94.8	3287	1781	716		
18H-6, 70–72 (CH)	166.5	98.6	3544	1302	388		
18H-6, 120–122	167	91.9	3507	1618	421	0.53	1.29
18H-7, 20–22 (CH)	167.5	96.4	3278	1333	463		
19H-1, 20–22	168.1	95.4	4108	1490	512		
19H-1, 70–72	168.6	94.1	3872	1839	827		
19H-1, 120–122	169.1	95.5	3856	1810	778	0.16	0.08
19H-2, 20–22	169.6	97.4	3412	1565	1630		
19H-2, 71–72	170.11	95.2	3330	1589	1540		
19H-2, 120–122	170.6	98.6	3084	1645	770		
19H-3, 20–22	171.1	96.6	3304	1343	1240		
19H-3, 70–72	171.6	98.5	3401	1541	1780		
19H-3, 120–122	172.1	97.5	3626	1399	1530		
19H-4, 20–22 (CH)	172.6	90.4	3722	3219	542	−0.03	0.61
19H-4, 70–72	173.1	92.5	3533	1649	990		
19H-4, 120–122 (CH)	173.6	95.4	3272	1411	784	0.15	0.61
19H-5, 20–22	174.1	95.7	3011	1432	585		
19H-5, 70–72	174.6	93.5	2890	1424	439		
19H-5, 120–122	175.1	96.1	2920	1421	467		
19H-6, 20–22	175.6	96.7	2829	1459	478		
19H-6, 70–72 (CH)	176.1	92.8	3072	3420	610		
19H-6, 120–122	176.6	95.3	2998	1501	643		
19H-7, 20–22 (CH)	177.1	95.7	3152	1354	533	0.25	0.85
20H-1, 20–22	177.7	91.3	3079	2655	609		
20H-1, 70–72	178.2	97.8	2865	1435	552		
20H-1, 120–122	178.7	96.3	2805	1508	664		
20H-2, 20–22 (CH)	179.2	95.6	3003	1400	498		
20H-2, 70–72 (CH)	179.7	97.9	3090	1379	541	0.1	0.7
20H-2, 120–122 (CH)	180.12	94.7	3330	1375	606		

Table 1 (continued).

Core, section, interval (cm)	Depth (mbsf)	$CaCO_3$ (wt%)	Mg (ppm)	Sr (ppm)	Na (ppm)	$\delta^{13}C$ (‰)	$\delta^{18}O$ (‰)
115-716B- (Cont.)							
20H-3, 20–22	180.7	94.7	3032	2294	1320		
20H-3, 70–72	181.2	95.2	3507	1234	862		
20H-3, 120–122 (CH)	181.7	95.1	3314	1522	748		
20H-4, 20–22 (CH)	182.2	93.3	3393	1736	1140	−0.07	0.05
20H-4, 120–122 (CH)	183.2	97.2	3114	1837	751		
20H-5, 20–22	183.7	96.3	3428	1354	669		
20H-5, 70–72	184.2	95.8	2787	1559	795		
20H-5, 120–122	184.7	96.4	2846	1523	566		
20H-6, 20–22	185.2	97.2	2712	1467	772	0.34	0.43
20H-6, 70–72	185.7	94.4	2894	1572	834		
20H-6, 120–122	186.2	97.7	2894	1769	517		
20H-7, 20–22	186.7	98.7	2255	1389	689		
20H-7, 70–72 (CH)	187.2	95.9	3026	1688	460	0.03	0.52
21H-1, 20–22	187.25	96.8	2645	1353	587	0.09	−0.47
21H-1, 70–72	187.75	97.9	2477	1573	746		
21H-1, 120–122	188.25	95.1	2740	1478	515		
21H-2, 20–22	188.75	97.4	2083	1435	613		
21H-2, 70–72	189.25	96.5	2681	1657	556		
21H-2, 120–122	189.75	94 8	2698	1614	616		
21H-3, 20–22	190.25	98-4	2590	1637			
21H-3, 70–72	190.75	95.7	2513	2018	985		
21H-3, 120–122	191.25	95.4	3008	2055	421	0.03	0.45
21H-4, 20–22	191.75	91.7	2921	1344	544		
21H-4, 70–72	192.25	94.7	2561	1667	716		
21H-4, 120–122 (1)	192.75	97.4	2446	1496	552		
21H-4, 120–122 (2)	192.75	98.6	2436	1476	592		
21H-4, 120–122 (3)	192.75	97.9	2477	1553	572		
21H-4, 120–122 (4)	192.75	96.6	2609	1556	570		
21H-5, 20–22	193.25	97.9	2528	1246	449	0.01	0.26
21H-5, 70–72	193.75	98.1	2406	1323	521		
21H-5, 120–122	194.25	97.2	2676	1359	552		
21H-6, 20–22	194.75	95.7	2723	1411	732		
21H-6, 70–72	195.25	94.2	2553	1729	707		
21H-6, 120–122	195.75	93.2	2741	1581	788	0.23	0.29
21H-7, 20–22	196.25	96.2	2739	1688	763		
22H-1, 20–22	197	88.6	2829	1878	607		
22H-1, 70–72	197.5	91.2	2901	1541	823		
22H-1, 120–122	198	93.1	2929	1488	567		
22H-2, 20–22 (CH)	198.5	93.4	3169	1171	739	0.1	0.93
22H-2, 70–72	199	93.6	3083	1408	1040		
22H-2, 120–122	199.5	94.5	2602	2034	961		
22H-3, 10–12 (*)	199.9	48.9	2406	17644	2640		
22H-3, 20–22	200	95.9	2351	2107	550	−0.07	−0.07
22H-3, 70–72	200.5	90.4	2742	1750	415		
22H-3, 120–122	201	93.4	2553	1649	771		
22H-4, 20–22	201.5	93.2	2782	1651	1010		
22H-4, 66–68 (*)	201.96	35.3	2413	55593	2370		
22H-4, 70–72	202	93.5	2461	1500	529	0.21	0.19
22H-4, 120–122	202.5	91.8	2531	1538	799		
22H-5, 20–22	203	94.5	2444	1623	817		
22H-5, 70–72	203.5	96.7	2478	1688	957		
22H-5, 120–122	204	92.9	2564	1649	760		
22H-6, 20–22	204.5	94.4	2399	1960	1010		
22H-6, 70–72	205	91.8	2227	2243	1230		
22H-6, 120–122	205.5	91.7	2457	1667	1180	0.09	−0.29
22H-7, 20–22	206	93.7	2501	1614	1150		
22H-7, 70–72	206.5	91.2	2583	1607	839		
23H-1, 20–22	206.7	84.5	2524	5983	1240	0.13	−0.31
23H-1, 70–72	207.2	94.3	2581	1580	911		
23H-1, 120–122	207.7	94.8	2544	1556	1010		
23H-2, 20–22	208.2	95.5	2593	1613	949	0.18	−0.03
23H-2, 70–72	208.7	94.2	2756	1614	823		
23H-2, 120–122	209.2	95.3	2629	1626	1010		
23H-3, 20–22	209.7	95.1	2504	1788	1060		
23H-3, 70–72	210.2	93.4	2371	1488	926		
23H-3, 120–122	210.7	91.8	2730	1619	944		
23H-4, 20–22	211.2	92.9	2666	1649	1240		
23H-4, 70–72	211.7	94.2	2421	1896	1120	0.12	−0.83
23H-4, 120–122	212.2	90.8	2529	1854	1310		
23H-5, 70–72	213.2	95.4	2038	1788	1320		
23H-5, 120–122	213.7	93.4	2061	1649	1040		
23H-6, 20–22	214.2	93.7	1975	1556	1160		
23H-6, 70–72	214.7	93.9	1964	1649	1110	0.06	−0.76
23H-6, 120–122 (1)	215.2	95.1	2012	1667	1220		
23H-6, 120–122 (2)	215.2	94.8	2012	1667	1260		
23H-6, 120–122 (3)	215.2	94.9	2018	1659	1250		
23H-6, 120–122 (4)	215.2	96.9	2007	1662	1210		

Table 1 (continued).

Core, section, interval (cm)	Depth (mbsf)	$CaCO_3$ (wt%)	Mg (ppm)	Sr (ppm)	Na (ppm)	$\delta^{13}C$ (‰)	$\delta^{18}O$ (‰)
115-716B- (Cont.)							
23H-7, 20–22	215.7	93.6	2286	1788	990		
24H-1, 20–22	216.3	94.4	2225	1572	1130	0.02	−0.23
24H-1, 70–72	216.8	95.2	2197	1580	1030		
24H-1, 120–122	217.3	95.8	2198	1675	835		
24H-2, 20–22	217.8	94.9	2292	1623	827		
24H-2, 70–72	218.3	93.7	2421	1636	722		
24H-2, 120–122	218.8	94.9	2018	1580	859		
24H-3, 20–22	219.3	90.4	2422	2533	697	0.45	0.15
24H-3, 70–72	219.8	93.5	2666	1665	685		
24H-3, 120–122	220.3	95.1	2718	1522	869		
24H-4, 20–22	220.8	97.1	2688	1434	660		
24H-4, 70–72	221.3	99.2	2328	1560	798		
24H-4, 120–122 (CH)	221.8	97.9	2453	1439	584	0.28	0.5
24H-5, 20–22	222.3	93.5	2235	2187	1020		
24H-5, 70–72	222.8	98.9	2378	1485	1640		
24H-5, 120–122	223.3	98.2	2456	1553	782		
24H-6, 20–22	223.8	97.1	2524	1536	886		
24H-6, 70–72	224.3	98.6	2047	1684	645		
24H-6, 120–122 (CH)	224.8	97.7	2350	1326	737	0.04	0.16
24H-7, 20–22	225.3	95.9	2559	1557	794		
24H-7, 70–72	225.8	95.1	2307	1501	695		
25H-1, 5–8 (CH)	225.85	96.7	2484	1364	897	0.35	0.61
25H-1, 20–22	226	95.8	2450	1421	550		
25H-1, 70–72	226.5	92.5	2329	1533	889		
25H-1, 120–122	227	95.1	2418	1422	769		
25H-2, 20–22	227.5	96.1	2272	1520	768		
25H-2, 70–72	228	93.1	2325	1577	877		
25H-2, 120–122	228.5	94.5	2457	1509	688		
25H-3, 20–22	229	95.6	2515	1499	1050	0.48	0.28
25H-3, 70–72	229.5	94.9	2436	1568	627		
25H-3, 120–122	230	95.1	2307	1443	611		
25H-4, 20–22	230.5	95.5	2360	1443	2600		
25H-4, 70–72	231	93.2	2349	1660	769		
25H-4, 120–122	231.5	95.1	2334	1602	706		
25H-5, 20–22	232	94.6	2360	1580	716		
25H-5, 70–72	232.5	96.1	2391	1520	856	0.4	0.03
25H-5, 120–122	233	96.5	2297	1527	612		
25H-6, 20–22	233.5	94.5	2261	1552	636		
25H-6, 70–72	234	98.1	2226	1413	600		
25H-6, 120–122	234.5	96.5	2260	1434	557		
25H 7, 20–22	235	96 4	2147	1597	695	0.21	−0.11
26H-1, 20–22	235.6	93-8	2346	1589	667		
26H-1, 70–72	236.1	94.8	2320	1631	646		
26H-1, 120–122	236.6	93.2	2411	1695	732	0.39	0.1
26H-2, 20–22	237.1	94.5	2389	1531	561		
26H-2, 70–72	237.6	96.8	2309	1367	512	0.08	0.02
26H-2, 120–122	238.1	96.6	2297	1478	643		
26H-3, 8-10 (*)	238.48	37.6	2069	52763	1550		
26H-3, 20–22	238.6	94.7	2039	1870	667		
26H-3, 70–72	239.1	93.2	2158	1738	732		
26H-3, 120–122	239.6	91.6	2327	2153	790		
26H-4, 20–22	240.1	92.8	2338	1804	673		
26H-4, 70–72	240.6	94.1	2468	1610	800		
26H-4, 120–122	241.1	94.1	2510	1488	508	0.16	0.25
26H-5, 20–22	242.6	96.9	2472	1357	485		
26H-5, 70–72 (1)	242.1	97.7	2320	1500	543		
26H-5, 70–72 (2)	242.1	94.5	2413	1531	752		
26H-5, 70–72 (3)	242.1	96.7	2383	1491	757		
26H-5, 70–72 (4)	242.1	96.9	2394	1512	764		
26H-5, 78–80 (CH)	242.18	93.3	2723	1738	1090	0.17	0.32
26H-5, 120–122 (CH)	242.6	94.3	2616	1500	502		
26H-6, 20–22	243.1	92.8	2637	1760	689		
26H-6, 70–72	243.6	92.9	2734	1937	786		
26H-6, 120–122	244.1	93.8	2833	1907	763		
26H-7, 20–22	244.5	94.9	2739	1981	821		
26H-7, 70–72	245.1	93.1	2723	1636	560		
27H-1, 20–22	245.3	93.7	2450	1762	630	0.31	0.2
27H-1, 70–72	245.8	98.2	2358	1489	549		
27H-1, 120–122	246.3	98.4	2234	1513	645		
27H-2, 20–22	246.8	96.7	2110	1491	619		
27H-2, 70–72	247.3	98.9	2038	1451	683		
27H-2, 120–122	247.8	96.6	1988	1517	594		
27H-3, 20–22	248.3	95.9	2038	1646	596	0.2	−0.02
27H-3, 70–72	248.8	98.2	2373	1504	620		
27H-3, 120–122	249.3	98.4	2154	1545	610		
27H-4, 20–22	249.8	91.5	2110	2722	703	0.02	−0.23
27H-4, 70–72	250.3	96.1	2178	1491	650		

Table 1 (continued).

Core, section, interval (cm)	Depth (mbsf)	$CaCO_3$ (wt%)	Mg (ppm)	Sr (ppm)	Na (ppm)	$\delta^{13}C$ (‰)	$\delta^{18}O$ (‰)
115-716B- (Cont.)							
27H-4, 120–122	250.8	95.8	2272	1577	768		
27H-4, 138-141 (*)	250.98	22.2	2207	71520	4660		
27H-5, 20–22	251.3	82.9	2811	1888	887		
27H-5, 70–72	251.8	95.6	2595	1599	675		
27H-5, 120–122	252.3	96.3	2645	1589	711		
27H-6, 20–22	252.8	95.5	2567	1613	612		
27H-6, 70–72	253.3	96.1	2621	1604	702		
27H-6, 120–122	253.8	95.8	2493	1725	596	0.36	0.22
27H-7, 20–22	254.3	93.5	2338	1644	817		
28H-1, 20–22	254.9	90.6	2073	2128	605		
28H-1, 70–72	255.4	96.2	2043	1589	774		
28H-1, 120–122	255.9	96.4	1944	1667	533	0.38	−0.02
28H-2, 20–22	256.4	93.6	2081	1769	678		
28H-2, 70–72	256.9	91.7	2073	2007	786		
28H-2, 120–122 (CH)	257.4	97.1	1961	1801	640	0.16	0.31
28H-3, 20–22	257.9	96.4	2173	1469	585		
28H-3, 70–72	258.9	96.5	2349	1499	726		
28H-4, 70–72	259.9	94.6	2334	1681	622		
28H-4, 120–122	260.4	96.3	2380	1613	570		
28H-5, 20–22	260.9	93.2	2554	1704	671	0.38	0.11
28H-5, 70–72	261.4	90.4	2739	1776	715		
28H-5, 120–122	261.9	91.7	2792	1786	638		
28H-6, 20–22	262.4	91.1	2810	1837	605		
28H-6, 70–72	262.9	95.3	2629	1746	638		
28H-7, 20–22	263.9	93.6	2643	1580	641		
28H-7, 70–72	264.4	96.4	2593	1520	560	0.39	0.37

Note: CH = chalk nodule and (*) = celestite nodule.

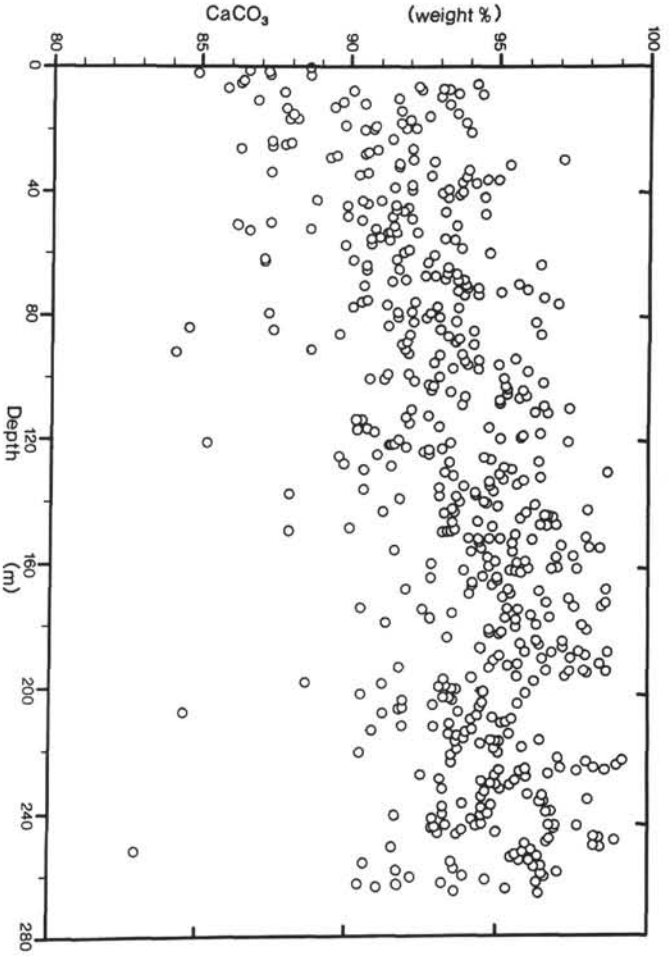

Figure 3. Calcium carbonate (wt%) as a function of sub-bottom depth.

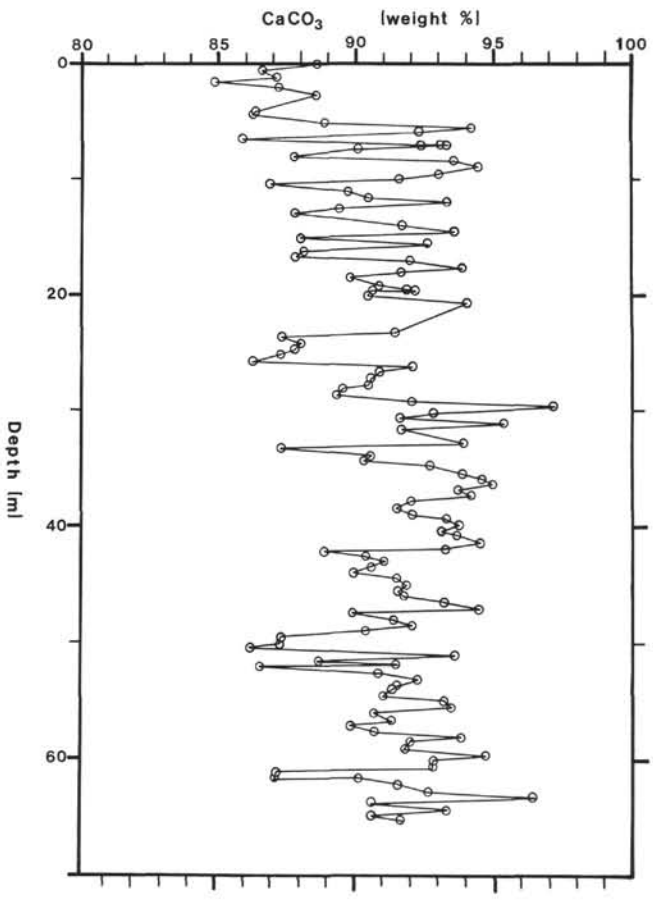

Figure 4. Calcium carbonate (wt%) for the upper 60 mbsf.

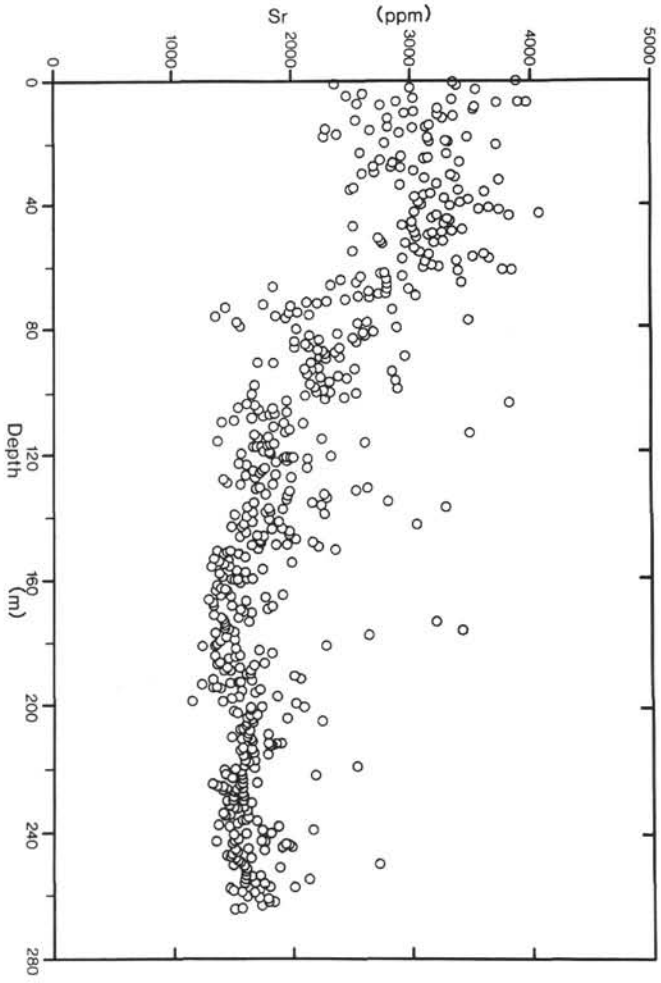

Figure 5. Strontium concentrations (ppm) in calcium carbonate as a function of sub-bottom depth.

sediments below 60 mbsf to dissolution of aragonite, HMC, and some biogenic LMC and reprecipitation of diagenetic LMC. Under these conditions, in which sulfate reduction is not excessive, dissolved strontium concentrations reach levels where pore waters are saturated or supersaturated with respect to celestite (Baker and Bloomer, 1988). At Site 716, at approximately 100 mbsf, dissolved strontium values reach maximum concentrations of about 500 μM (Swart and Burns, this volume). The shallowest celestite nodule was recovered at 111.6 mbsf.

As illustrated in Figures 5 and 7, strontium and sodium concentrations behave in a similar manner, although strontium is much more variable than sodium. The sodium values gradually decrease from a maximum of 2000 ppm at the top of the core to about 1300 ppm at 60 mbsf. At 60 mbsf, sodium concentrations abruptly decline to values of approximately 1000 ppm or less. An exception occurs at about 210 mbsf, where concentrations increase to 1200 ppm and then decrease again. As with strontium, we believe the monotonic decrease in sodium is the result of the dissolution of biogenic calcium carbonate and the reprecipitation of diagenetic LMC.

Sodium concentrations in the upper 60 m are not as variable as strontium values in the same interval, although sodium concentrations are known to be enriched in biogenic aragonite and HMC (i.e., shallow-water algae) over LMC (foraminifers and coccoliths) (Busenberg and Plummer, 1985). We suggest that this may be related to the different chemical behavior of the two elements. Busenberg and Plummer (1985) have shown experimentally that sodium does not substitute for calcium in lattice sites in calcite but probably occupies interstitial positions in the crystal lattice. They have shown that the amount of incorporated sodium seems to be limited by the number of crystal defects, which, in turn, is a function of crystal growth rate and would certainly also be a function of crystal age.

Magnesium concentrations behave very differently than strontium and sodium. Magnesium values range from about 2000 to 6000 ppm (Fig. 8). The variability in the upper 40 mbsf is mostly attributable to the increased input of HMC from the bank-tops. The first two peaks of magnesium coincide with peaks of HMC. Below 32 mbsf, HMC is no longer present; therefore, HMC cannot explain the increases in magnesium. Below 40 mbsf, these cycles display a lower amplitude fluctuation, with values ranging from ~2000 to 4000 ppm. High magnesium values do not appear to be confined to the nodules but are also found in sediment between more lithified layers.

Carbon and Oxygen Isotopes

Oxygen and carbon isotope values of selected bulk samples are shown in Figures 9 and 10 and compiled in Table 1. The $\delta^{18}O$ values range from $-1.5‰$ to $1.3‰$, whereas $\delta^{13}C$ values range from $-0.1‰$ to $1.0‰$. Generally, $\delta^{18}O$ and $\delta^{13}C$ covary downcore. Both show positive excursions at about 60 and 140 mbsf and negative excursions at about 20, 100, and 190 mbsf. The $\delta^{18}O$ and $\delta^{13}C$ curves also display similarity to the magnesium curve. Values of $\delta^{18}O$ and $\delta^{13}C$ seem to increase in intervals of increased concentrations of magnesium and in intervals of increased induration, but neither $\delta^{18}O$ nor $\delta^{13}C$ are significantly

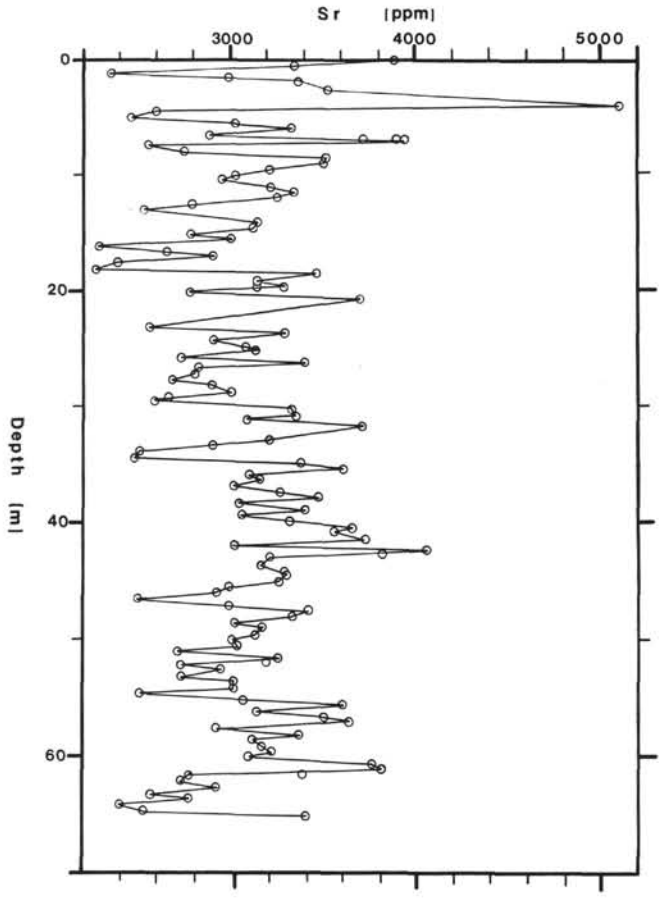

Figure 6. Strontium concentrations (ppm) in calcium carbonate for the upper 60 mbsf.

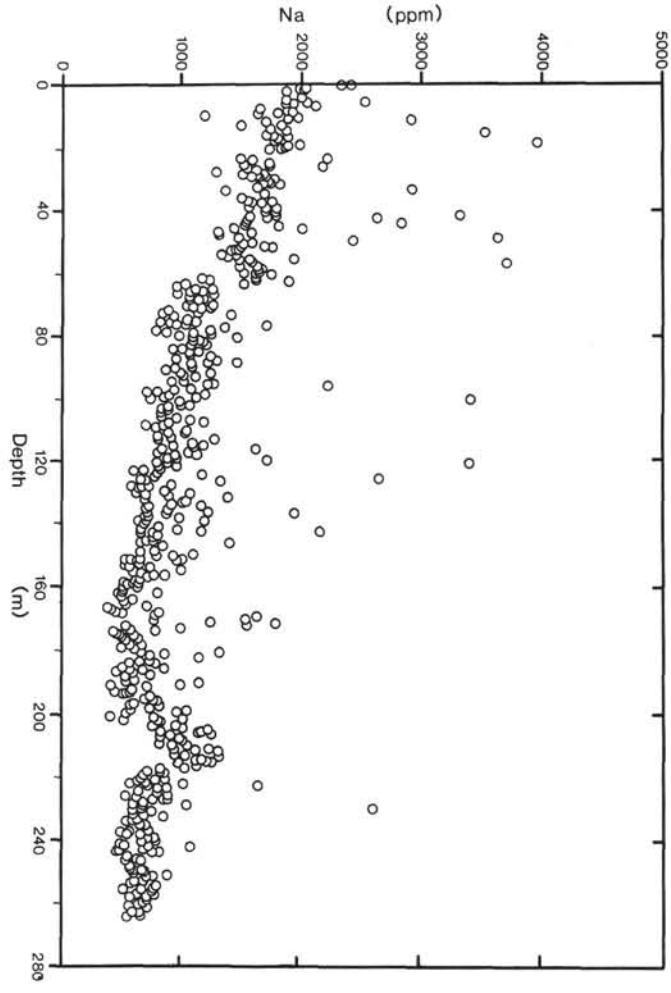

Figure 7. Sodium concentrations (ppm) in calcium carbonate as a function of sub-bottom depth.

higher in discrete chalk nodules relative to neighboring sediments (Figs. 9 and 10).

Scanning Electron Microscopy

The scanning electron microscope (SEM) photomicrographs in Figure 11 illustrate the textural differences in sediments from near the seafloor in Site 716 compared with chalk horizons from the lower part of the core. Figure 11A is a nannofossil ooze from interglacial Stage 1 at 0.1 mbsf (as defined by Droxler et al., this volume). Figure 11B shows sediment from glacial Stage 2 at 0.7 mbsf. This sample is considerably coarser and consists primarily of planktonic foraminifers. Figure 11C, from a chalk layer at 155.8 mbsf, shows rhombs of calcite cement. Figure 11D, a chalk from 257.4 mbsf near the bottom of the core, illustrates the compacted nature of the chalks from this depth.

DISCUSSION

Site 716 is unusual among all deep-sea carbonate drill sites because of its rapid lithification and shallow occurrence of chalks. In this study, we focus on the timing and nature of cementation that produced these chalks. Specifically, we will resolve whether or not the chalks formed by (1) seafloor or near-seafloor cementation, (2) burial diagenesis at an accelerated pace relative to deep-sea pelagic carbonates, or (3) a combination of both mechanisms.

Seafloor Cementation

In the Bahamas, seafloor cements are common in Pleistocene periplatform carbonate sediments (Wilbur, 1978; Mullins et al., 1980; Kiefer, 1983; Slowey, 1985; Haddad, 1986). These Bahamian cements usually occur in glacial-age sediments or in glacial-to-interglacial transitions when shallow-water carbonate saturation is higher (because of decreased water depth and, therefore, increased water temperatures) and sedimentation rates are lower. Likewise, we might expect seafloor cementation in the Maldives to be more important during glacial stages than during interglacial stages. Contrary to this expectation, no chalks were found at Site 716 throughout the Pleistocene. They only occur in Pliocene and older sediments. This observation supports the hypothesis that the chalks formed during burial diagenesis.

If the chalk horizons formed at or near the sediment-water interface, then they would be expected to be isotopically heavier in oxygen and carbon than adjacent uncemented zones. Using a temperature of 10°C at a water depth of 500 m (obtained from GEOSECS Stations 447 and 448) (Weiss et al., 1983), an estimate that Indian Ocean Intermediate Water at salinity of 35.00 g/kg has a $\delta^{18}O$ of seawater = 0.0‰ (SMOW) and applying oxygen isotope fractionation factors between calcium carbonate and water as reported by O'Neil et al. (1969), we calculate equilibrium $\delta^{18}O$ of calcium carbonate cement forming on the seafloor as 0.9‰ (PDB). The oxygen isotopic values of bulk sediments in cemented intervals should be shifted from the assumed original isotopic composition of the sediment part way toward this predicted cement value. Figure 9 shows that, except for the three shallowest chalks, most chalks are not shifted significantly from the values of neighboring less cemented sediments.

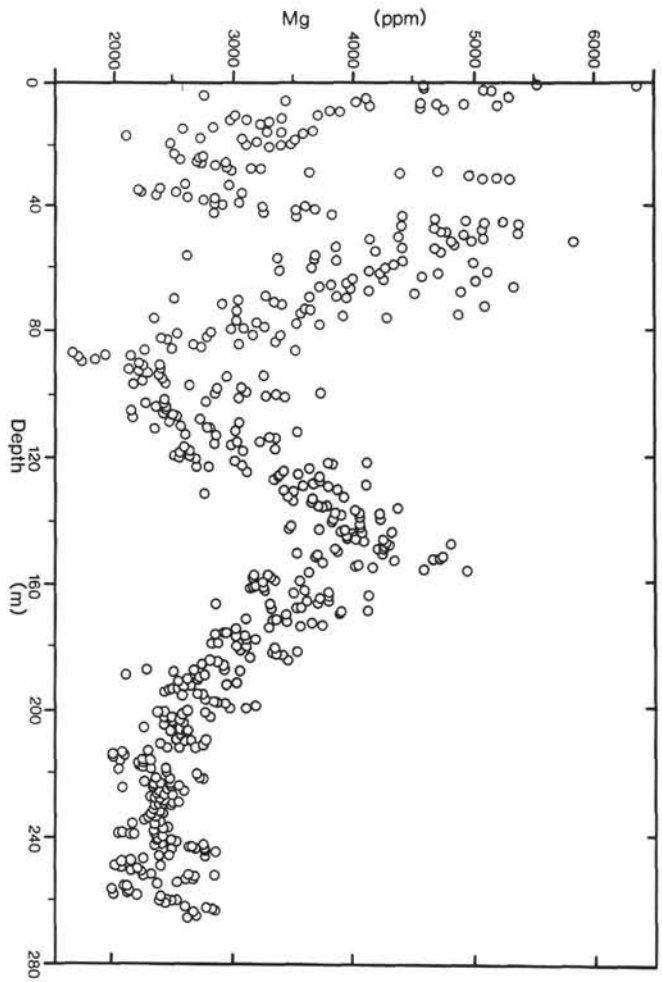

Figure 8. Magnesium concentrations (ppm) in calcium carbonate as a function of sub-bottom depth.

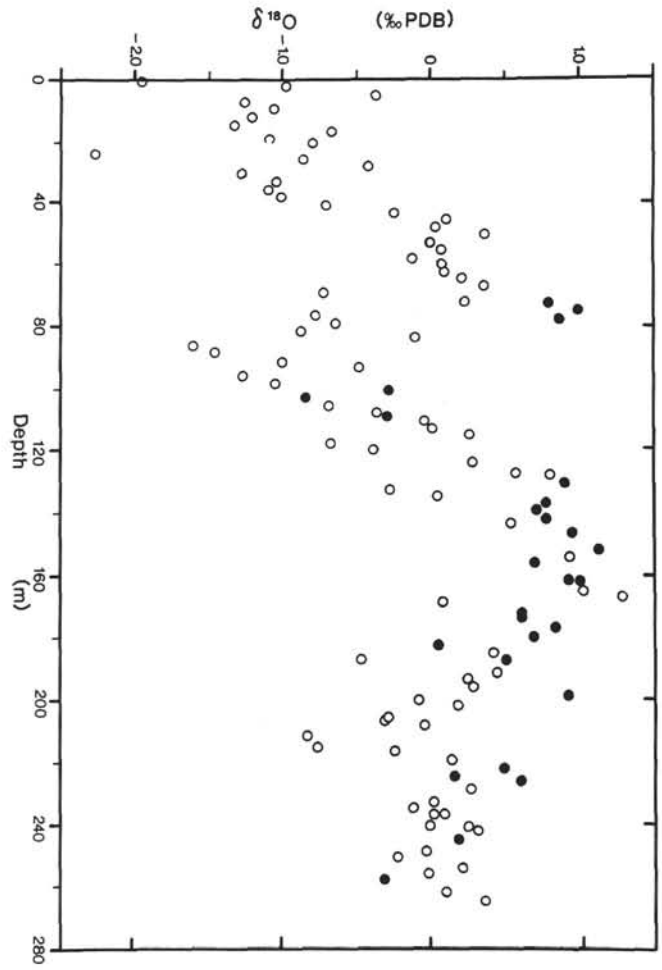

Figure 9. $\delta^{18}O$ as per mil (‰) deviations from PDB as a function of sub-bottom depth. Solid circles are chalks.

Using carbon isotope fractionation factors between calcium carbonate and dissolved bicarbonate reported by Emrich et al. (1970), $\delta^{13}C$ values of dissolved inorganic carbon from GEOSECS Stations 447 and 448 (Kroopnick, 1985) and a temperature of 10°C from the same sites (Weiss et al., 1983), we calculate an equilibrium $\delta^{13}C$ of 1.9‰ (PDB) for calcium carbonate cements forming at the seafloor. Carbon isotopic values of sediments in the cemented intervals should also be shifted part way between the assumed original isotopic composition of the sediment and predicted cement values. The $\delta^{13}C$ values of chalks shown in Figure 10 are not significantly shifted toward predicted seafloor values. Thus, neither carbon nor oxygen isotopic compositions nor the depth distribution of the chalks support their origin as seafloor cements.

Burial Diagenesis

The evidence for calcium carbonate cementation during burial diagenesis is convincing. We believe that the downcore changes in mineralogy—the rapid disappearance of HMC and the more gradual decrease in aragonite—as well as the monotonic decrease of strontium and sodium are a result of the ongoing process of burial diagenesis. Droxler et al. (this volume) have shown that there is high-frequency mineralogical variation in the upper 60 mbsf because of variations in the primary depositional record. We think that the primary record has been substantially modified by diagenesis, especially in older sediments. The downcore decrease of strontium in the sediment and the corresponding downcore increase of dissolved strontium in the pore waters (Swart and Burns, this volume) prove that recrystallization of biogenic aragonite and calcite to inorganic calcite during burial diagenesis is occurring. Likewise, the formation of celestite nodules requires the recrystallization of biogenic calcium carbonate to increase pore-water-dissolved strontium concentrations sufficiently to allow celestite saturation (Baker and Bloomer, 1988).

Magnesium concentrations at Site 718 vary widely and do not display, in any straightforward way, trends like those observed during pelagic carbonate diagenesis (Baker et al., 1982; Renard, 1986). When LMC recrystallizes during burial diagenesis in deep-sea monomineralic calcitic oozes, normally there is a slight downcore increase of magnesium in the carbonate solids. Such changes are of much smaller magnitude and occur at far slower rates than those observed in periplatform oozes at Site 716. The HMC present in periplatform carbonate sediments converts to LMC much more rapidly, causing a decrease in the magnesium content of the sediments. Correspondingly, a small downcore increase of magnesium in the pore waters might also be expected throughout this zone. Pore-water data at Site 716 (Swart and Burns, this volume) do reveal a slight, possibly significant, increase of dissolved magnesium in the upper 40 mbsf.

Below the zone containing HMC, there are two intervals of highly elevated magnesium values in the bulk sediment. The magnesium content of these intervals has two likely origins: either these zones are composed of a small amount (about 10%)

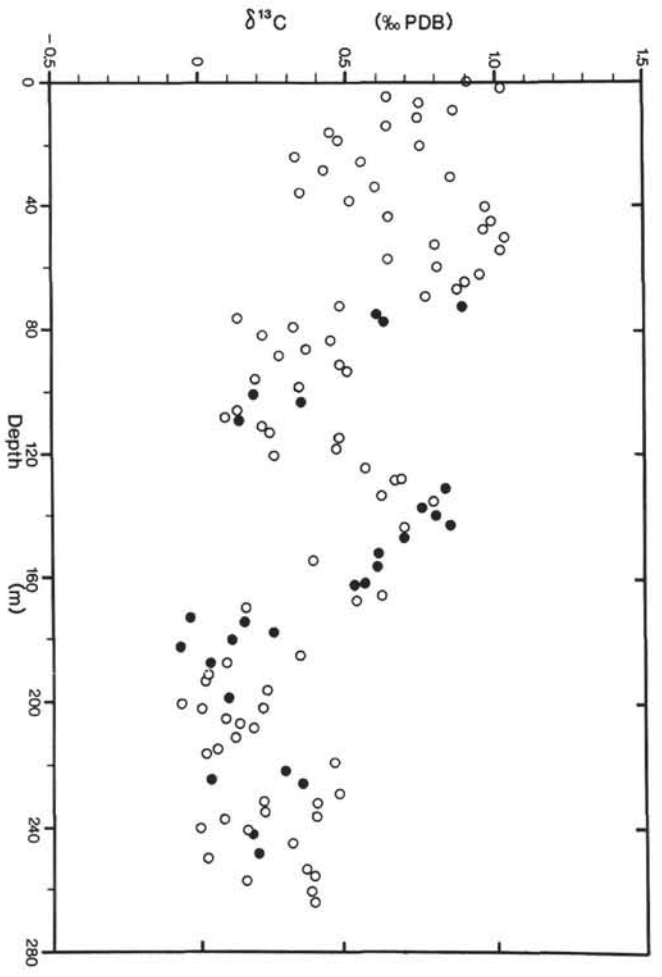

Figure 10. $\delta^{13}C$ as per mil (‰) deviations from PDB as a function of sub-bottom depth. Solid circles are chalks.

of HMC cement or they are composed of a large amount of only mildly enriched LMC cement. Because XRD results reveal no HMC below 32 mbsf, the second hypothesis is favored. If we assume that these intervals contain about 30% cement, then these cements are composed of about 3–4 mol% magnesium. Figures 2 and 8 show that magnesium and aragonite generally covary downcore. Consequently, these two magnesium peaks could represent a vestige of the former presence of HMC, coincident with the aragonite highs in the original sediment. This implies that the originally high percentage of HMC and its subsequent conversion to LMC in these layers of sediment resulted in accelerated rates of recrystallization. The resultant recrystallized LMC retained much of the original magnesium and, therefore, is mildly enriched relative to less-cemented intervals. Thus, magnesium contents in older periplatform carbonate sediments may also be expected to record past elevated inputs of HMC, and possibly aragonite, as well as past high stands of sea level.

As previously noted, $\delta^{13}C$ and magnesium covary below 40 mbsf. Therefore, the coherent variations in $\delta^{13}C$ may also represent variations in sedimentary input from the banks. Bank-derived biogenic aragonite, such as green algae, is enriched in ^{13}C, usually ranging from 2.0‰ to 5.0‰ (PDB) (Milliman, 1974). Figures 2 and 10 show that positive excursions of $\delta^{13}C$ are associated with increases in aragonite. This relationship is especially apparent between 120 and 160 mbsf. Because $\delta^{13}C$ covaries with the aragonite content of the present sediments, $\delta^{13}C$ variations may also reflect an isotopic signature inherited from formerly present aragonite and HMC recrystallized to LMC.

Differences between $\delta^{18}O$ of pelagic and shallow water components are generally much less however, (Milliman, 1974) and cannot explain the variations in $\delta^{18}O$ at this site. It is also well known that the original $\delta^{13}C$ record is better preserved than the original $\delta^{18}O$ record, because most of the carbon in sediments is found in calcium carbonate whereas most of the oxygen is in water. If we assume a geothermal gradient of 25°C/km for Site 716, then recrystallization during burial diagenesis must have occurred between ~10° and 17°C. Therefore, carbonate sediments equilibrated with colder waters than waters in which they formed. Consequently, an increase of $\delta^{18}O$ is expected to occur during isotopic equilibration, and intervals of greater recrystallization should be characterized by positive shifts of $\delta^{18}O$. Therefore, at increased burial depths, $\delta^{18}O$ values increasingly reflect the process of recrystallization and increasingly covary with the magnesium and $\delta^{13}C$ curves.

CONCLUSIONS

Stabilization of metastable carbonates at Site 716 is rapid. HMC disappears and is reprecipitated as LMC within 1.1 Ma, whereas most aragonite has disappeared and is converted to LMC by 2.5 Ma and is completely gone by 6 Ma. The youngest celestites (in equilibrium with modern-day pore waters) occur in sediments of approximately 3.4 Ma, coincident with the sub-bottom depth of the maximum rate of decrease of solid strontium concentrations. Strontium concentrations in carbonate solids decrease with depth in response to burial diagenesis. Sodium concentrations in carbonate solids rapidly decrease with depth and are also controlled by burial diagenesis.

Magnesium concentrations vary widely. In sediments younger than 1.1 Ma, magnesium concentration variations are controlled by the amount of HMC present. Intervals of increased magnesium values in sediments older than 1.1 Ma are a result of episodes of cementation during burial diagenesis. These intervals are controlled by the former higher abundance of metastable platform-derived aragonite and HMC. Carbon isotopes record these changes in sedimentary input from shallow-water banks. Primary carbon isotopic compositions are retained despite extensive burial diagenesis. Oxygen isotopes also record a primary paleoceanographic signal in sediments younger than approximately 2 Ma, but the $\delta^{18}O$ values of sediments older than 2 Ma (below 60 mbsf) increasingly reflect equilibration of carbonates with cold pore waters during diagenetic dissolution and reprecipitation. These conclusions have important implications for the diagenesis of ancient shallow-water limestones:

1. Biogenic HMC recrystallizes faster than biogenic aragonite, which recrystallizes faster than biogenic LMC. Rates of recrystallization at this site are 1 Ma for HMC and 2.5–6 Ma for aragonite.
2. Magnesium is, at least partially, retained during the recrystallization of HMC in marine pore fluids. Hence, high magnesium values found in ancient limestones may be caused by an original high content of HMC. In contrast, strontium does not seem to be retained much during the dissolution of aragonite and reprecipitation of LMC.
3. In periplatform carbonate sediments or limestones, carbon isotopic highs may be the result of increased inputs of shallow-water-derived aragonitic components. These values are retained during marine burial diagenesis. Oxygen isotopic changes in the sediments record the presence of sub-bottom cements. It is expected that oxygen isotopic values will be overprinted by later cementation.

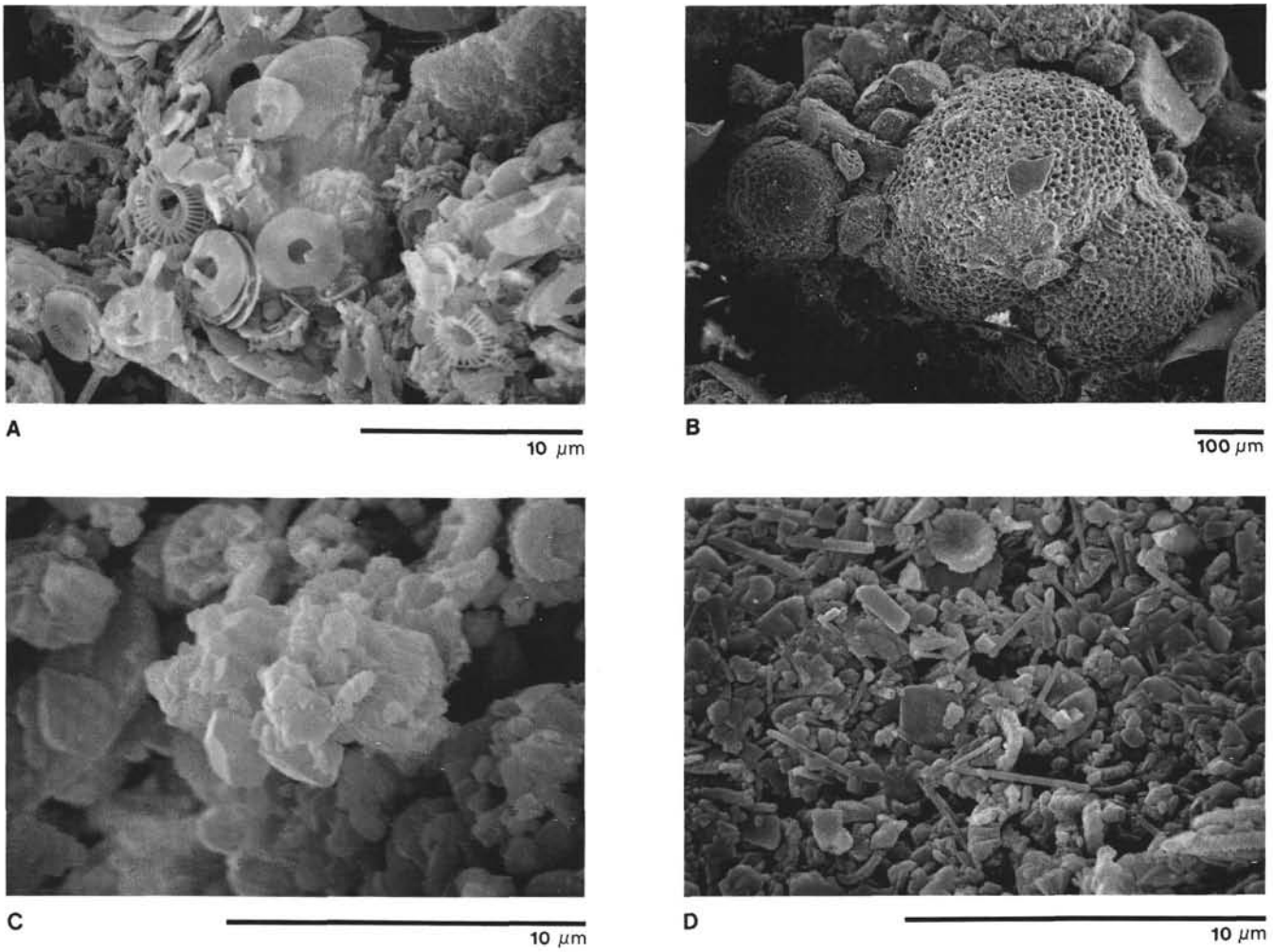

Figure 11. SEM photomicrographs. **A.** Nannofossil ooze (0.1 mbsf). **B.** Planktonic foraminifers (0.7 mbsf). **C.** Chalk horizon showing calcite cement (155.8 mbsf). **D.** Chalk horizon (257.4 mbsf).

ACKNOWLEDGMENTS

We thank the crew and the rest of the shipboard technical and scientific parties, especially the co-chief scientists, J. Backman and R. A. Duncan. The help of all these people was essential for the present study. We thank A. Droxler and G. Haddad for their help in sampling and providing preliminary data and reviews. We also thank M. Malone for assistance in sampling. The comments of two anonymous reviewers were very helpful. We acknowledge the support by USSAC and National Science Foundation Grant No. OCE-87-18382 to P. A. Baker.

REFERENCES

Backman, J., Duncan, R. A., et al., 1988. *Proc. ODP, Init. Repts.,* 115: College Station, TX (Ocean Drilling Program).

Baker, P. A., 1981. The diagenesis of marine carbonate sediments: experimental and natural observations [Ph.D. dissert.]. Univ. California, San Diego.

Baker, P. A., and Bloomer, S. H., 1988. The origin of celestite in deep-sea carbonate sediments. *Geochim. Cosmochim. Acta,* 52:335–340.

Baker, P. A., Gieskes, J. M., and Elderfield, H., 1982. Diagenesis of carbonates in deep-sea sediments—evidence from Sr/Ca ratios and interstitial dissolved Sr^{2+} data. *J. Sediment. Petrol.,* 52:71–82.

Boardman, M. R., and Neumann, A. C., 1984. Sources of periplatform carbonates: Northwest Providence Channel, Bahamas. *J. Sediment. Petrol.,* 54:110–1123.

Boardman, M. R., Neumann, A. C., Baker, P. A., Dulin, L. A., Kenter, R. J., Hunter, G. E., and Kiefer, K. B., 1986. Bank-top response to Quaternary fluctuations in sea level recorded in periplatform sediments. *Geology,* 14:28–31.

Burns, S. J., and Neumann, A. C., 1987. Pelagic sedimentation on an inactive gullied slope, Northwest Providence Channel, Bahamas. *Mar. Geol.,* 77:277–286.

Busenberg, E., and Plummer, L. N., 1985. Kinetic and thermodynamic factors controlling the distribution of SO_4^{2-} and Na^+ in calcites and selected aragonites. *Geochim. Cosmochim. Acta,* 49:713–725.

Dix, G. R., and Mullins, H. T., 1988a. A regional perspective of shallow-burial diagenesis of deep-water periplatform carbonates from the Northern Bahamas. *In* Austin, J. A., Jr., Schlager, W., et al., *Proc. ODP, Sci. Results,* 101: College Station, TX (Ocean Drilling Program), 279–302.

_____, 1988b. Rapid burial diagenesis of deep-water carbonates: Exuma Sound, Bahamas. *Geology,* 16:680–683.

Droxler, A. W., Schlager, W., and Wallon, C. C., 1983. Quaternary aragonite cycles and oxygen-isotope record in Bahamian carbonate ooze. *Geology,* 11:235–239.

Droxler, A. W., Bruce, C. H., Sager, W. W., and Watkins, D. H., 1988. Pliocene-Pleistocene variations in aragonite content and planktonic

oxygen-isotope record in Bahamian periplatform ooze, Hole 633A. *In* Austin, J. A., Jr., Schlager, W., et al., *Proc. ODP, Sci. Results,* 101: College Station, TX (Ocean Drilling Program), 221–244.

Emrich, K., Ehhalt, D., and Vogel, J., 1970. Carbon isotope fractionation during the precipitation of calcium carbonate. *Earth Planet. Sci. Lett.,* 8:363–371.

Gealy, E. L., Winterer, E. L., and Moberly, R., Jr., 1971. Methods, conventions, and general observations. *In* Winterer, E. L., Riedel, W. R., et al., *Init. Repts. DSDP,* 7, Pt. 1: Washington (U.S. Govt. Printing Office), 9–26.

Haddad, G. A., 1986. A study of carbonate dissolution, stable isotope chemistry and minor element composition of pteropods and forams deposited in the Northwest Providence Channel, Bahamas during the past 500,000 years [M.S. thesis]. Duke Univ., Durham, NC.

Kiefer, K., 1983. Quaternary climatic cycles recorded in the isotopic record of periplatform pelagic deposition [M.S. thesis]. Duke Univ., Durham, NC.

Kier, J. S., and Pilkey, O. H., 1971. The influence of sea-level changes on sediment carbonate mineralogy, Tongue of the Ocean, Bahamas. *Mar. Geol.,* 11:189–200.

Kroopnick, P., 1985. The distribution of ^{13}C of ΣCO_2 in the world oceans. *Deep-Sea Res.,* 32:57–84.

Milliman, J. D., 1974. *Marine Carbonates* (2nd ed.): Berlin-Heidelberg-New York (Springer-Verlag).

Mullins, H. T., Neumann, A. C., Wilbur, R. J., and Boardman, M. R., 1980. Nodular carbonate sediment on Bahamian slopes: possible precursors to nodular limestones. *J. Sediment. Petrol.,* 50:117–131.

Mullins, H. T., Wise, S. W., Jr., Gardulski, A. F., Hinchey, E. J., Masters, P. M., and Siegel, D. I., 1985a. Shallow subsurface diagenesis of Pleistocene periplatform ooze: northern Bahamas. *Sedimentology,* 32:473–494.

Mullins, H. T., Wise, S. W., Jr., Land, L. S., Siegel, D. I., Masters, P. M., Hinchey, E. J., and Price, K. R., 1985b. Authigenic dolomite in Bahamian periplatform slope sediment. *Geology,* 13:292–295.

O'Neil, J. R., Clayton, R. E., and Mayeda, T. K., 1969. Oxygen isotope fractionation in divalent metal carbonates. *J. Chem. Physics,* 51: 5547–5558.

Renard, M., 1986. Pelagic carbonate chemostratigraphy (Sr, Mg, ^{18}O, ^{13}C). *Mar. Micropaleontol.,* 10:117–164.

Schlager, W., and James, N. P., 1978. Low-magnesian calcite limestones forming at the deep-sea floor Tongue of the Ocean, Bahamas. *Sedimentology,* 25:675–702.

Slowey, N. C., 1985. Fine-scale acoustic stratigraphy of Northwest Providence Channel, Bahamas [M.S. thesis]. Univ. North Carolina, Chapel Hill, NC.

Swart, P. K., and Guzikowski, M., 1988. Interstitial-water chemistry and diagenesis of periplatform sediments from the Bahamas, ODP Leg 101. *In* Austin, J. A., Jr., Schlager, W., et al., *Proc. ODP, Sci. Results,* 101: College Station, TX (Ocean Drilling Program), 363–380.

Weiss, R., Broecker, W., Craig, H., and Spencer, D., 1983. *GEOSECS Atlas. Indian Ocean Expedition: Hydrographic Data* (Vol. 5): Washington (U.S. Govt. Printing Office).

Wilbur, R. J., 1976. Petrology of submarine-lithified hardgrounds and lithoherms from their deep flank environment of the little Bahama Bank (Northeast Straits of Florida) [M.S. thesis]. Duke Univ., Durham, NC.

Date of initial receipt: 12 June 1989
Date of acceptance: 5 January 1990
Ms 115B-184